Experimental and numerical transport AC losses in a four-strand Roebel cable bifilar stack

Wenjuan Song[1,2]**, Zhenan Jiang**[2] ⬤**, Mike Staines**[2]**,**
Rodney A Badcock[2] ⬤ **and Jin Fang**[1]

[1] School of Electrical Engineering, Beijing Jiaotong University, Haidian, Beijing 100044, People's Republic of China
[2] Robinson Research Institute, Victoria University of Wellington, PO Box 33436, Lower Hutt 5046, New Zealand

E-mail: zhenan.jiang@vuw.ac.nz

CrossMark

Abstract

REBCO Roebel cables are promising candidates for bifilar coils (or non-inductive coils) in large scale high temperature superconducting resistive type fault current limiters (SFCLs), as they enable large current-carrying capability in conjunction with low AC loss. Here we report transport AC loss measurement results in two Roebel cable bifilar stacks (RBS) with different vertical spacing between the turns assembled from a straight 4/2 (four 2 mm width strands) Roebel cable. We also report two-dimensional finite element method AC loss simulation results using the H-formulation in the RBSs, in two parallel bifilar stacks (TPBS) which have the same geometrical dimensions as the RBS with 0.284 mm spacing (g) but have unequal current distribution between the conductors composing the stacks, and in an equivalent bifilar stack (EBS) comprising four 4 mm wide conductors while keeping identical vertical geometrical dimensions with the RBS with $g = 0.284$ mm but has unequal current distribution between the conductors. We show that the measured transport AC loss values in the RBS with $g = 0.284$ mm are approximately one fifth of those in the parent straight 4/2 Roebel cable due to cancellation of the perpendicular magnetic field components in the bifilar stack, and also show the AC loss in RBSs increases with increasing g. We then show the calculated transport AC loss values in the RBS with $g = 0.284$ mm are approximately one third of the values in the TPBS and EBS when $I_{t,turn}/I_{c0,cable} > 0.6$, where $I_{t,turn}$ is the current amplitude for upper or lower turn of the bifilar stacks and $I_{c0,cable}$ is nominal I_c value for the 4/2 Roebel cable. We numerically demonstrate that the result is caused by flux flow loss in the inner conductors in the TPBS and EBS due to unequal current distributions in conductors. Roebel cables show clear advantage over simple vertical stacks for SFCL applications in terms of AC loss.

Keywords: transport AC loss, bifilar Roebel cable stack, H-formulation, unequal current distribution

(Some figures may appear in colour only in the online journal)

1. Introduction

Large scale resistive type superconducting fault current limiters (SFCLs) require high current-carrying capacity and low AC loss which could be achieved through a bifilar coil structure [1–3]. There are several candidates for high current-carrying capacity: CORCs [4–6], vertical stacks [7–10], and Roebel cables [11–14]. However it is hard to wind bifilar coils using CORCs due to their round shape. On the other hand, simple vertical stacks will have unequal current sharing between the conductors composing the stacks, which may cause large AC loss in the coil windings unless they are transposed at coil level

[15, 16]. In comparison, Roebel cables are ideal candidates for high rating SFCLs, because of their capability of achieving equal current sharing due to their transposed nature, and flat shape which enables bifilar coil winding. On the other hand, it has the disadvantages of the added manufacturing steps of strand cutting and cable assembly. Using present strand cutting methods about 50% of the high temperature superconducting (HTS) conductor is wasted, adding considerably to the cost. Looking to the future, there is the prospect that this situation will improve. The availability of wide-strand feed material, 100 mm or wider, coupled with the possibility of laser cutting Roebel strand using a nested strand profile to minimize waste have the potential to reduce the cost penalty of manufacturing Roebel cables. Compared to winding parallel wire, in addition to guaranteed current sharing, a Roebel cable does have the advantage of winding a single conductor, compared with the complication of winding tapes in a stack using multiple pay-off reels. Up to now, there have been limited reports on AC loss in HTS conductors due to equal or unequal current sharing between conductors either in Roebel cables or simple stacks [17, 18].

In our previous work, we measured AC loss in bifilar stacks with various current-canceling and current-additive vertical stacks of up to six wires [10]. In this case, equal current sharing was imposed by serial connection of the wires. Therefore, the measurement results could not show the influence of unequal current sharing between the wires and hence represent an ideal case in terms of AC loss for vertical stacks, with equal current sharing assumed to be achieved by coil level transposition [16].

In this work, we measured transport AC loss in Roebel bifilar stacks (RBS) composed of two vertically stacked 4/2 (four 2 mm wide strands) Roebel cables carrying opposed currents. Two different vertical gaps *g* were used between the two cables, 0.284 and 1.03 mm, in order to explore the effect on the AC loss of the reduced magnetic field cancellation with increased separation. Data was obtained at three different frequencies. The AC loss of the parent 4/2 Roebel cable from which the stack was built was also measured. The measured results were compared with numerical values calculated from a two-dimensional (2D) finite element method (FEM) model using the *H*-formulation. A range of conductor geometries were simulated. To explore the effect of unequal current sharing the RBS were compared with simulation results for two parallel bifilar stacks (TPBS) with the same geometrical dimensions as the RBS but with the current allowed to distribute unequally between the conductors of the top and bottom half of the stack. AC loss was also calculated for an equivalent bifilar stack (EBS) comprising four 4 mm wide conductors with the same vertical geometrical dimensions as the RBS but with unequal current distribution between the inner and outer conductors.

2. Measurement and numerical methods

2.1. Measurement method

The 4/2 Roebel cable, with a length of 410 mm, was reassembled from a 9/2 Roebel cable used in our previous work [12]. The strands for the cable were punched from 12 mm
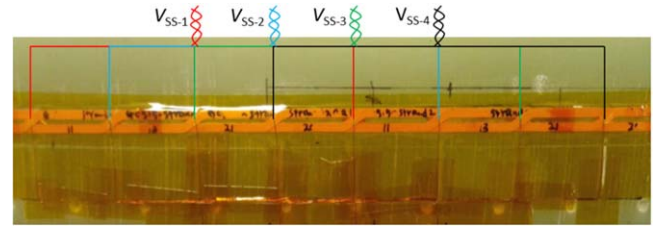
Figure 1. Voltage loop arrangement for transport AC loss in the straight 4/2 Roebel cable.

Table 1. Critical current of each strand composing the Roebel cable and the RBSs.

|	SS-1	SS-2	SS-3	SS-4	Cable
Self-field I_c (A)	47.0	47.3	47.6	47.1	189.0[a]
I_c in the 4/2 Roebel cable (A)	41.1	41.4	40.7	40.8	164
I_c in RBS with $g = 0.284$ mm (A)	40.1	N.M.	N.M.	39.4	159.1
I_c in the RBS with $g = 1.03$ mm (A)	40.6	N.M.	N.M.	40.8	162.8

[a] In the modeling, $I_{c0,cable} = 189.0$ A was used for self-field I_c of the Roebel cable, which is the summation of the self-field I_c values of the four strands. $I_{c0,strand} = 47.3$ A was used as the self-field I_c of each strand which was obtained by $I_{c0,cable}/4$.

wide SuperPower tape (SCS12050) with a 20 μm copper stabilization layer on both sides. The transposition length is 90 mm and the horizontal gap between the strands in the Roebel cable is 1 mm. All strands were insulated individually with a 20 μm thick epoxy acrylate polymer layer on both sides. Self-field strand I_c values were remeasured in order to make sure there was no deterioration in I_c values. Table 1 lists the measured self-field I_c values of the strands which are very similar, with maximum deviation of less than $\pm 1\%$.

Transport AC loss in the 4/2 Roebel cable was measured by connecting each strand in series in order to avoid unequal current distribution in each Roebel strand caused by the slight difference in contact resistance values in parallel connected Roebel strands [19]. The current direction in each strand was made the same with current jumpers arranged symmetrically around the Roebel cable [12]. If the electrical property of each Roebel strand is the same and uniform over the length, then transport AC loss in the Roebel cable can be measured using only one of the four rectangular voltage loops shown in figure 1, and the loss can be given as [20]

$$Q_t = \frac{I_{cable}V_{loss}}{df} = \frac{4I_{SS-i}V_{SS-i}}{df} \quad \text{where } V_{loss} = V_{SS-i}, \quad (1)$$

where SS-*i* (*i* = 1, 2, 3, and 4) denotes *i*th Roebel strand; V_{loss} is the in-phase loss voltage of the cable, V_{SS-i} is the in-phase voltage in rms obtained from *i*th rectangular voltage loop with respect to the phase of the strand current; I_{cable} is the Roebel cable current in rms which is the summation of the current values in the four Roebel strands; *d* is the distance between the voltage taps, here *d* = 90 mm; *f* is the frequency of the transport current. Because the Roebel strands have very close
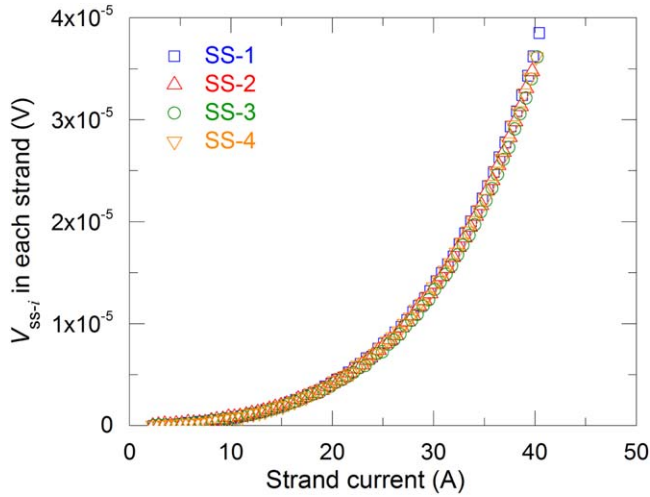
Figure 2. V_{SS-i} values plotted as a function of Roebel strand current at 27.74 Hz.

strand I_c values as shown in table 1, the measured V_{SS-1}, V_{SS-2}, V_{SS-3}, and V_{SS-4} values plotted as a function of the Roebel strand current have perfect agreement as shown in figure 2. The result proves that transport AC loss can be measured using only one rectangular voltage loop. In this work, V_{loss} value was obtained from $\sum_{i=4}^{4} V_{SS-i}/4$ for data analysis.

Two RBSs were assembled from the same straight 4/2 Roebel cable by bending the cable in the middle to get the upper and lower turns of the RBSs as shown in figure 3(a). The overlapping sections of the RBSs are approximately two pitch lengths allowing for voltage loop arrangement and current terminations. Figures 3(b) and (c) show the schematics of the cross-section of the RBSs with vertical spacing, $g = 0.284$ mm and 1.03 mm, respectively. The Roebel strands were connected in series. Current jumpers were arranged in order to achieve opposite current direction in the upper and lower turns of the RBSs. The bending section of the stack was supported by a polyvinyl chloride cylinder which has a diameter of 27 mm. The bending diameter is big enough to prevent any strand I_c deterioration [21]. It is worth noting that the cross-over sections of the Roebel cable within the upper turn of the RBSs sit exactly on the cross-over sections of the cable within the lower turn of the RBSs. Only two rectangular loops were arranged from each turn of the RBSs based on the measurement method for the straight Roebel cable: one on SS-1 in the lower turn of the RBSs and the other one on SS-4 in the upper turn of the RBSs. The voltage loop arrangements can be seen from figure 3(a). Transport AC loss in the RBSs per cycle per length per turn, $Q_{t,bifilar}$, can be given as [10, 22]

$$Q_{t,\,bifilar} = \frac{I_{cable}(V_{SS-1} + V_{SS-4})}{2df} = \frac{2I_{SS-1}(V_{SS-1} + V_{SS-4})}{df}. \tag{2}$$

Two lock-in amplifiers were used for the measurements: one for registering the phase and amplitude of the Roebel strand current; the other for registering in-phase voltage in each voltage loop. All measurements were carried out at 77 K.
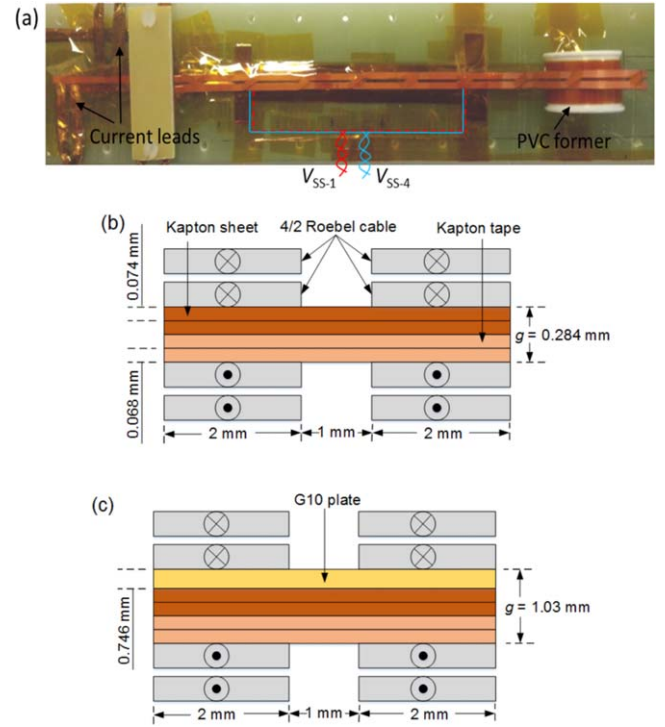
Figure 3. (a) Sample arrangement for transport AC loss measurement in the RBSs, (b) schematic of the cross-section of the RBS with $g = 0.284$ mm, (c) schematic of the cross-section of the RBS with $g = 1.03$ mm. Sections depict the geometry between cross-over sections.

2.2. Numerical method

A 2D FEM model employing *H*-formulation implemented using COMSOL was built to study the AC loss characteristic of the bifilar stacks and straight Roebel cable [23]. Structured mesh and edge element were used in the model [24, 25].

State variables in the 2D model are the horizontal magnetic field component, H_x and the vertical magnetic field component, H_y. The superconductor property is given by the following nonlinear relationship

$$E = E_c \left(\frac{J}{J_c(B)} \right)^n, \tag{3}$$

where index $n = 30$, critical electrical field $E_c = 10^{-4}$ V m^{-1}, and $J_c(B)$ is the critical current density dependence on magnetic field.

A modified Kim model [26] was adopted for the $J_c(B)$ relation which provides J_c when the superconductor is subjected to a combination of parallel and perpendicular magnetic fields

$$J_c(B) = J_{c0} \left(1 + \frac{\sqrt{k^2 B_{//}^2 + B_\perp^2}}{B_0} \right)^{-\alpha}, \tag{4}$$

where J_{c0} is the critical current density in the self-field. In a realistic coated conductor sample, B_0 is a constant depending on the material, and here we used $B_0 = 42.6$ mT; $B_{//}$ and $B_\perp$ are the parallel and perpendicular components of a local magnetic field, respectively; $\alpha = 0.7$ and $k = 0.3$ are
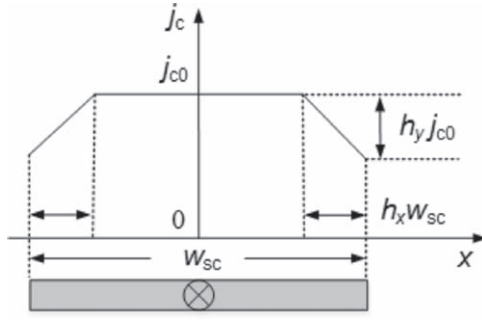
Figure 4. Schematic of non-uniform lateral J_c distribution along conductor width (not drawn to scale).

Figure 5. Schematic of one quarter model for RBS and TPBS.

Figure 6. Schematic of the EBS comprising four 4 mm wide coated conductors, keeping the same vertical dimensions as the RBS with $g = 0.284$ mm and TPBS.

constants determined by the I_c–B curves of the conductor measured under applied magnetic field [27].

In coated conductors, J_c values at the conductor edges are normally degraded due to slitting or punching processes [28]. Therefore, a trapezoidal shaped lateral J_c distribution was taken into account in this work [29, 30]. Figure 4 shows the schematic of non-uniform lateral J_c distribution along conductor width. Equation 5 assumes j_{c0} is reduced symmetrically towards tape edges [31], where the coordinate x runs along the conductor width w_{sc}. The non-uniformity is characterized by two parameters: h_x defines the width portion of the tape with reduced J_c at each edge; and h_y represents the portion of reduced J_c at the tape edge compared to the critical current density at the tape center, j_{c0}. Publications have shown that h_x can vary from 5%–10%, and h_y varies from 20%–80%, depending on fabricating process and manufacturer [31]. The parameters used in this work are $h_x = 7.5\%$ and $h_y = 50\%$, which gave the best agreement between measured and calculated AC loss results in both the 4/2 Roebel cable and the RBS with $g = 0.284$ mm, shown later in figures 12 and 13

$$J_{c0} = j_{c0} \begin{cases} 1 & \text{if} |x| \leqslant \dfrac{1-h_x}{2} w_{sc} \\ 1 - h_y - \left(\dfrac{|x|}{w_{sc}} - \dfrac{1}{2} \right) \dfrac{h_y}{h_x} & \text{if} |x| > \dfrac{1-h_x}{2} w_{sc} \end{cases}. \quad (5)$$

j_{c0} can be obtained from the measured $I_{c0,strand}$ shown in table 1 and expressed as

$$j_{c0} = \frac{I_{c0}}{w_{sc} h_{sc} (1 - h_x h_y)}. \quad (6)$$

It is worth noting that there could be other factors which could influence simulation results such as n value, variation in electric properties along longitudinal directions, self-field effect when extracting J_c (B) curves which we did not consider in this work [32]. Therefore, we do not claim the simulation results considering both $J_c(B)$ and $J_c(x)$ presented in the work are perfect.

Previous publications established that Roebel cable can be modeled as two parallel stacks carrying the same current in each strand [11, 12, 33, 34]. Based on the symmetry of the
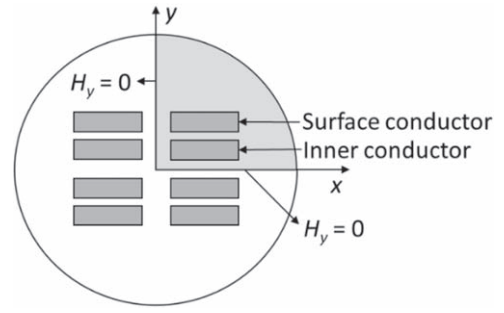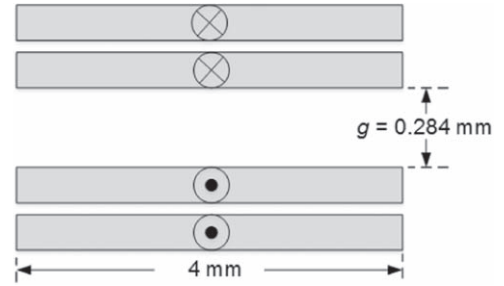
cross-section of the RBS and TPBS as shown in figure 3(b), only one quarter of the geometry was simulated as illustrated in figure 5. We define 'surface conductor' and 'inner conductor' as shown in the figure. The boundary condition of $H_y = 0$ was set on both the x-axis and y-axis (y-component of magnetic field is equal to zero on these two axes) [25].

It is challenging to wind a coil winding using the TPBS comprising eight 2 mm wide conductors due to the difficulty in handling the TPBS. It is much easier to use the equivalent bifilar stack, EBS, comprising four 4 mm width coated conductors as shown in figure 6 for coil winding as was done in a previous SFCL [2]. The EBS has the same equivalent superconductor width and vertical spacing between the neigbouring conductors as the RBS with $g = 0.284$ mm and TPBS. As with the RBS and TPBS, only a one quarter model was simulated as shown in figure 7.

The followings are some additional information for the numerical calculations. In this work, the structured meshes for the 2 mm wide superconductor layers have 150 horizontal and two vertical elements, respectively [24]. Transport currents were imposed by means of integral constraints on the current density J over the cross-section of the conductors. One integral constraint per conductor was applied to satisfy the requirement of equal current distribution in RBS while one integral constraint over the total cross-section of the 'surface conductor' and 'inner conductor' in the TPBS/EBS was applied to ensure current in the conductors can freely be distributed between the two conductors [3, 25].
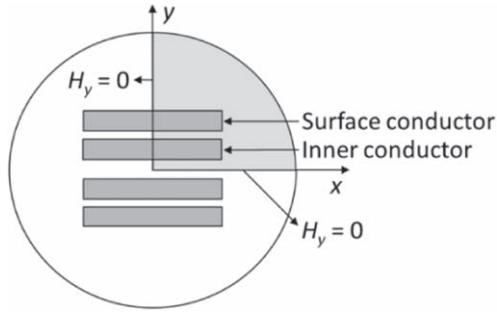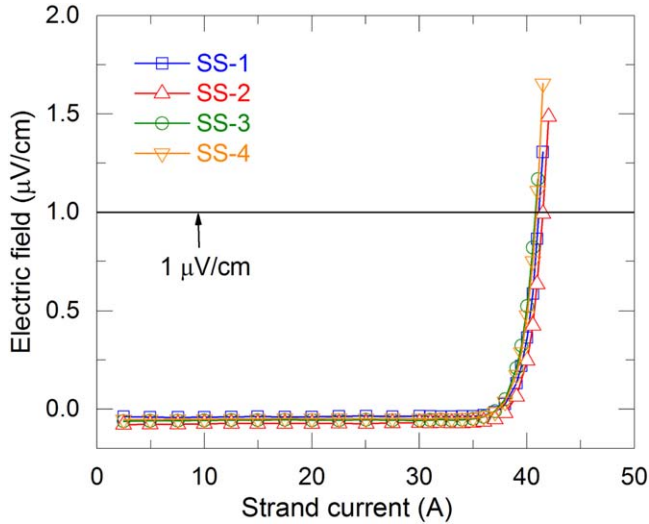
Figure 7. Schematic of a quarter model of the EBS.

Figure 8. *E–I* curves of the Roebel strands in the 4/2 Roebel cable measured from four voltage taps using serial connection.

3. Experimental and numerical results

3.1. DC critical current measurement in the 4/2 Roebel cable

Figure 8 shows *E–I* curves from each Roebel strand in the 4/2 Roebel cable. It is worth noting that the measurement was carried out by connecting the Roebel strands in series. The curves collapse on to one common curve due to the serial connection and close self-field I_c values of the Roebel strands [12]. Table 1 lists the measured strand I_c values and the summation of the measured values, 164 A, gives the Roebel cable I_c value.

The Roebel strand I_c measurement was also carried out in the two RBSs. Table 1 also lists the results. In this table, $I_{c0,cable}$ is nominal cable I_c which is the simple summation of the self-field strand I_c values. The averaged self-field strand I_c value of 47.3 A was used as $I_{c0,strand}$ in the numerical model. The two strand I_c values in the RBS with $g = 0.284$ mm measured from SS-1 and SS-4 agree with each other. In the bifilar arrangement, we expect slightly increased strand I_c values. However, the measured strand I_c values are slightly smaller than those in the straight cable. This might be due to the overlapping of the cross-over sections of the Roebel cable in the upper and lower turns of the RBS as mentioned in the previous section which caused superposition of magnetic
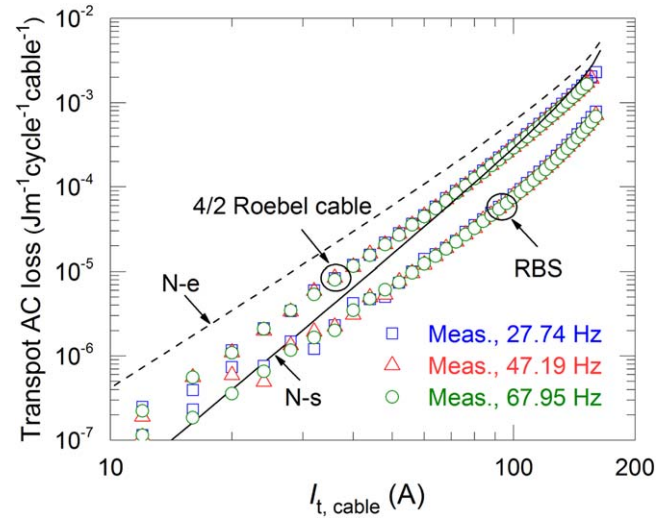

Figure 9. Comparison of measured transport AC loss results between the 4/2 Roebel cable and the RBS with $g = 0.284$ mm at different frequencies.

fields and it in turn could reduce the strand I_c. The two strand I_c values in the RBS with larger spacing improved slightly as shown in the table. This is expected due to the reduced influence of the magnetic field superposition with larger separation.

3.2. AC loss measurement

Figure 9 shows the measured transport AC loss in the straight 4/2 Roebel cable at three different frequencies plotted as a function of the Roebel cable current. In the figure, the theoretical transport AC losses based on Norris-ellipse (N-e) and Norris-strip (N-s) models [35] using the measured cable I_c value of 164 A are plotted together. The measured AC loss values fall between N-e and N-s in the low current region and has good agreement with N-s at high current amplitudes. The results at different frequencies agree well from one to other, confirming the hysteretic nature of the measured loss. The loss characteristics are similar to the results shown in our previous reports [12, 36].

In the figure, the measured transport AC losses, normalized by the number of cables, in the RBS with $g = 0.284$ mm at three different frequencies are plotted together. Similarly there is hardly frequency dependence in the results. The measured AC loss values were reduced significantly by the bifilar arrangement. We attribute this to the cancellation effect of the perpendicular magnetic field components between the upper and lower turns of the bifilar stack [10].

In figure 10, the AC loss reduction ratio at 27.74 Hz in the RBS with $g = 0.284$ mm over the isolated straight Roebel cable, $(Q_{cable} - Q_{g=0.284})/Q_{cable}$, where $Q_{g=0.284}$ is the transport AC loss in the RBS with $g = 0.284$ mm, is plotted as a function of the cable current. At the cable current amplitude, $I_{t,cable}$, ranging from 40 to 160 A, the reduction ratios are between 65% and 75%, while at $I_{t,cable} = 20$ A, the AC loss reduction ratio is less than 40% as seen in the figure. We
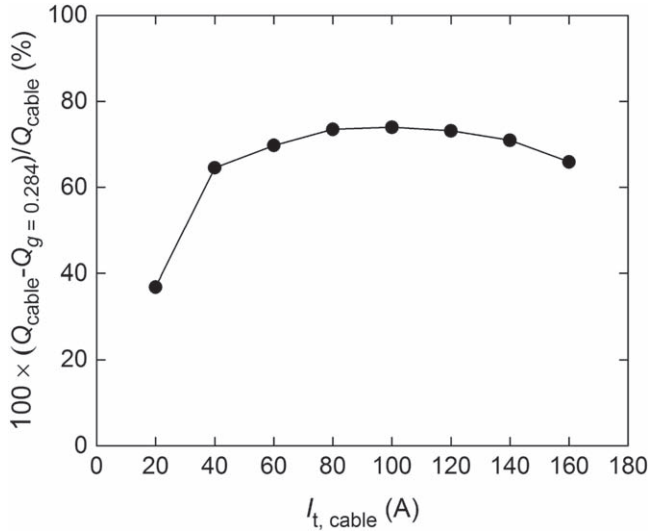
Figure 10. AC loss reduction ratio at 27.74 Hz in the RBS with $g = 0.284$ mm over the isolated straight 4/2 Roebel cable, $(Q_{\text{cable}} - Q_{g = 0.284})/Q_{\text{cable}}$.
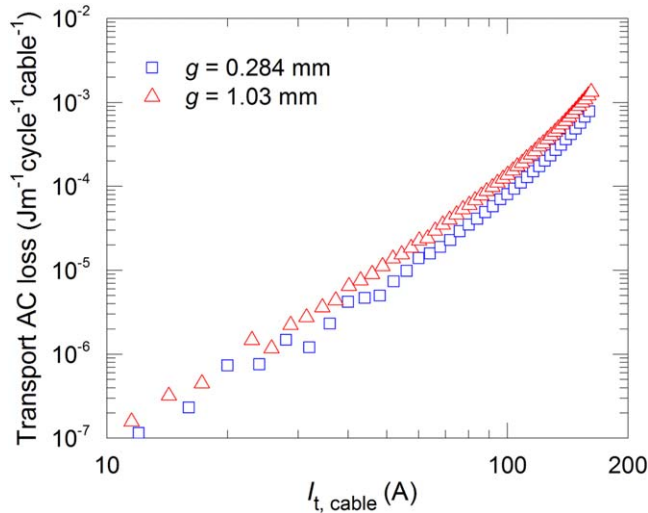

Figure 11. Comparison of transport AC loss values in the RBSs with $g = 0.284$ mm and 1.03 mm at 27.74 Hz.

attribute this to the scattering of measured value at $I_{\text{t,cable}} = 20$ A shown in figure 9.

Figure 11 plots the measured transport AC loss results in the RBS with $g = 1.03$ mm, $Q_{g = 1.03}$ as a function of the cable current and compares it with $Q_{g = 0.284}$ at 27.74 Hz. AC loss increased with the increase of the spacing between upper and lower turns of the RBS due to less cancellation of the perpendicular magnetic field components, showing similar dependence on spacing observed in non-Roebel vertical bifilar stacks [10]. The ratios expressed as $(Q_{g = 1.03} - Q_{g = 0.284})/Q_{g = 0.284}$ are between 60% and 70% at cable current amplitudes ranging from 60–160 A.

3.3. Numerical results

In figure 12, the calculated transport loss values in the straight 4/2 Roebel cable are compared with the experimental results
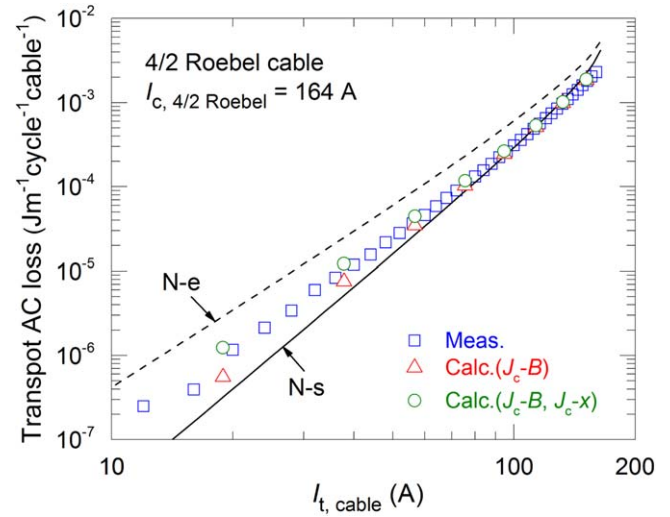
Figure 12. Calculated AC losses in the 4/2 Roebel cable at 27.74 Hz. Calc. $(J_c - B)$ and Calc. $(J_c - B, J_c - x)$ denote the calculated AC loss results taking into account only the dependence J_c on the magnetic field and those taking account both the dependence J_c on both the magnetic field and the lateral J_c distribution, respectively.

at 27.74 Hz. In this figure, Calc. $(J_c - B)$ and Calc. $(J_c - B, J_c - x)$ denote the calculated AC loss results taking account only the dependence J_c on the magnetic field and those taking account both the dependence J_c on both the magnetic field and the lateral J_c distribution, respectively. We attribute the better agreement between the experimental results and Calc. $(J_c - B, J_c - x)$ than between the experimental results and Calc. $(J_c - B)$ at low current amplitudes to the non-uniform lateral J_c distribution [15]. The results reconfirm that transport AC losses in a Roebel cable can be obtained by modeling two parallel stacks where each conductor carries the same current [11, 12, 33]. At $I_{\text{t,cable}} = 94.52$ A ($I_t/I_{c0,\text{cable}} = 0.5$), the difference between experimental and Calc. $(J_c - B, J_c - x)$ is 6.5%.

Figure 13 compares the calculated and measured transport AC losses in the RBS with $g = 0.284$ mm at 27.74 Hz. Calc. $(J_c - B)$ and Calc. $(J_c - B, J_c - x)$ were defined as the same as the above. Again, Calc. $(J_c - B, J_c - x)$ have better agreement with the experimental results. At $I_{\text{t,cable}} = 94.52$ A ($I_t/I_{c0,\text{cable}} = 0.5$), the difference between the measured values and Calc. $(J_c - B, J_c - x)$ is 15%.
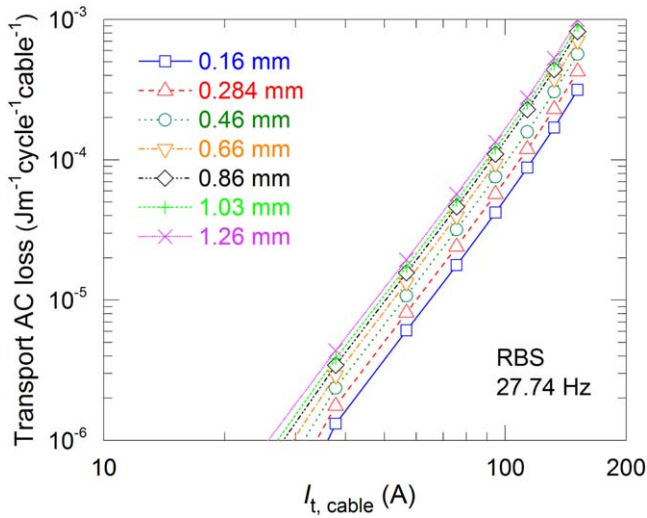
Figure 14 compares Calc. $(J_c - B, J_c - x)$ in the RBSs with various g values from 0.16 to 1.26 mm. The AC loss in the RBSs increased with increasing g value. The AC loss values in the RBS with $g = 1.26$ mm are approximately three times the AC loss values in the RBS with $g = 0.16$ mm.

3.4. Effect of equal and unequal current distribution on AC loss

Coils wound with Roebel cables can achieve equally distributed current in each strand due to the continuously transposed structure of the cable [14]. On the other hand, simple vertical stacks without transposition are a convenient option for winding coils with large current-carrying capacities [2]. However, conductors in simple vertical stacks without
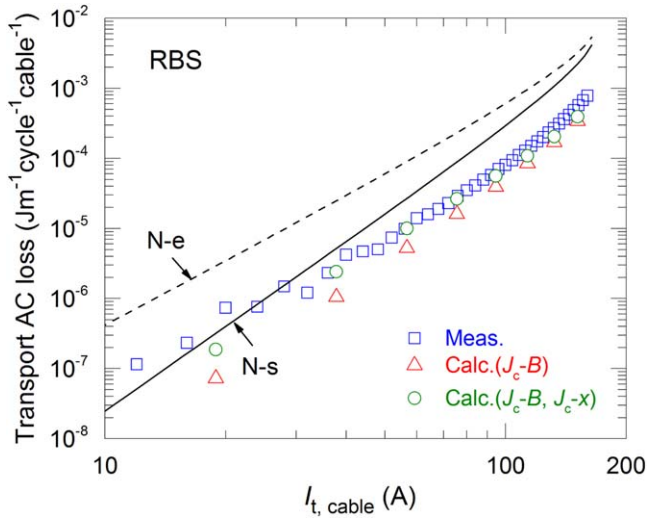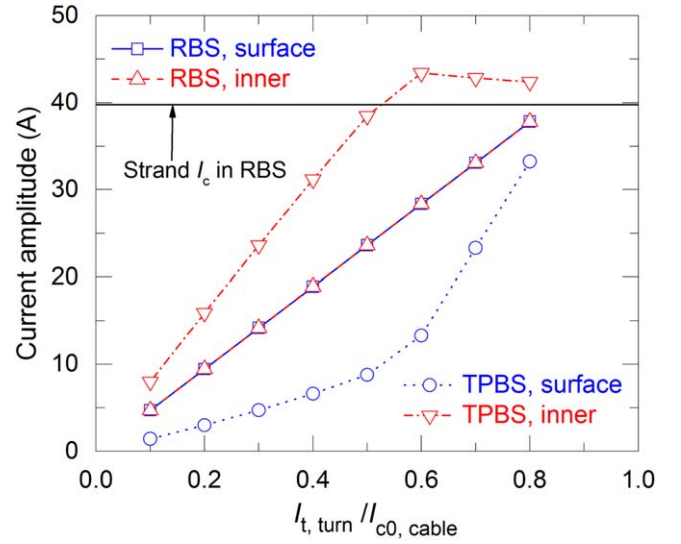
Figure 13. Calculated AC losses in bifilar Roebel cable assembly ($g = 0.284$ mm) at 27.74 Hz compared with the measured results.

Figure 14. Comparison of calculated transport AC loss values in the RBSs with various g values from 0.16 to 1.26 mm. The lines are guides to the eye.

Figure 15. The evolution of current distribution in the 'surface conductor' and 'inner conductor' with increasing $I_{t,turn}$ in the RBS and TPBS. The strand I_c, 39.8 A, in the RBS in this figure is obtained by averaging the measured two strand I_c values shown in table 1.

transposition feel different in a magnetic field either in a straight stack form or in coil windings, and this results in unequal current sharing between the conductors. In order to investigate the current sharing patterns on AC loss characteristics in the non-transposed bifilar stacks, we carried out numerical calculations on the RBS with $g = 0.284$ mm with the same current in each strand, and in TPBS which has the same geometrical dimensions as RBS but with unequal current sharing between conductors, as well as in EBS comprising four 4 mm wide conductors with the same vertical spacing as the RBS but with unequal current distribution between the conductors.

Figure 15 shows the calculated current distributions in the 'surface conductor' and 'inner conductor' of the RBS and TPBS defined in figure 5 for various $I_{t,turn}/I_{c0,cable}$ values when $\omega t = 3\pi/2$, where $I_{t,turn}$ is the current amplitude for the

4/2 Roebel cable in the RBS and the current amplitude for the upper or lower half stack in the TPBS and EBS. It is worth noting that 'surface conductor' and 'inner conductor' could represent the other three pairs of conductors in the RBS and TPBS due to the symmetry. The 'surface conductor' and 'inner conductor' carry exactly the same current for the whole current range in the RBS. In the TPBS, with increasing $I_{t,turn}$, current in both the 'surface conductor' and 'inner conductor' increases linearly only until $I_{t,turn}/I_{c0,cable}$ reaches 0.5. The 'surface conductor' in the TPBS carries much less current than the 'inner conductor' and the difference between the current values is the largest when $I_{t,turn}/I_{c0,cable}$ is around 0.5. The current in the 'inner conductor' in the TPBS saturates from $I_{t,turn}/I_{c0,cable}$ approximately 0.6 and becomes slightly smaller with increasing $I_{t,turn}$. On the other hand, current in the 'surface conductor' in the TPBS becomes larger from $I_{t,turn}/I_{c0,cable} > 0.5$. This clearly indicates current redistribution between the two conductors through the terminals in the TPBS and the behavior could be explained using a circuit model described in figure 16. E.g. at $I_{t,turn}/I_{c0,cable} = 0.3$ and 0.7, the current amplitudes of the 'surface conductor' and 'inner conductor' in the TPBS are 4.73 A, 23.62 A, and 23.32 A, 42.85 A, respectively.

The circuit comprises four branches in the RBS and TPBS: the 'surface conductor' and 'inner conductor' in the upper half; the 'surface conductor' and 'inner conductor' in the bottom half which carry opposite current with their upper counterpart conductors due to symmetry. Branch 1 refers to the upper 'surface conductor', branch 2 refers to upper the 'inner conductor', branch 3 refers to the bottom 'inner conductor', branch 4 refers to the bottom 'surface conductor'. Considering current direction in each conductor, the equations for the circuit for the 'surface conductor' and 'inner
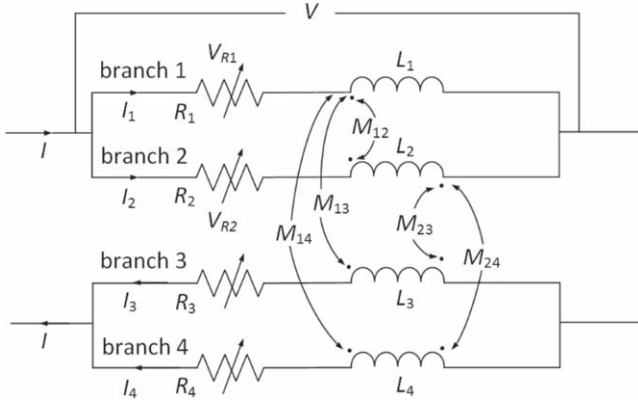
Figure 16. Circuit model for the 'surface conductor' and the 'inner conductor' for RBS and TPBS.

conductor' can be written as follows

$$
\begin{aligned}
V &= (R_1 + j\omega L_1)I_1 + j\omega M_{12}I_2 - j\omega M_{13}I_3 \\
&\quad - j\omega M_{14}I_4 \\
&= (R_2 + j\omega L_2)I_2 + j\omega M_{21}I_1 - j\omega M_{23}I_3 \\
&\quad - j\omega M_{24}I_4,
\end{aligned} \tag{7}
$$

where minus is due to opposite current direction in the two branches; R_1 and R_2 are resistance values defined by the E–J relationship of the conductors; L_1, L_2 are self-inductance values of the two conductors, I_1, I_2, I_3, and I_4 are current values in each branch; I is total current for the two branches; and M_{12}, M_{13}, M_{14}, M_{21}, M_{23}, M_{24} are the mutual inductance of branches defined as in figure 16; V, V_{R_1}, V_{R_2}, are voltages appearing at the terminals of the two branches, R_1, and R_2. Because of symmetry, $I_1 + I_2 = I_3 + I_4$; $I_1 = I_4$ and $I_2 = I_3$; $M_{13} = M_{24}$. In addition, $L_1 = L_2 = L$ due to the same geometry and material of the conductors.

When the 4/2 Roebel cable is used, each Roebel strand is electrically equivalent, and hence all parameters in the two branches in figure 16 are the same. Therefore, I_1 and I_2 are always the same in this case. However, in the TPBS, when I is small, R_1 and R_2 values are zero, then we can derive the ratio between I_1 and I_2 from equation (7) as follows

$$
\begin{aligned}
\frac{I_1}{I_2} &= \frac{j\omega L + j\omega(M_{13} - M_{23} - M_{12})}{j\omega L + j\omega(M_{24} - M_{14} - M_{21})} \\
&= \frac{L + M_{13} - M_{12} - M_{23}}{L + M_{24} - M_{21} - M_{14}},
\end{aligned} \tag{8}
$$

where $L + M_{13} - M_{12} = L + M_{24} - M_{21}$. M_{23} is bigger than M_{14} due to the stronger interaction between the 'inner conductors' than is the case for the 'surface conductors'. To support the previous point, figure 17 shows magnetic field distribution around the 'surface conductor' and the 'inner conductor' in TPBS at $I_{t,turn}/I_{c0,cable} = 0.7$. The 'inner conductor' is exposed to parallel or weakened perpendicular magnetic field mainly due to more thorough cancellation of perpendicular magnetic field components with the other 'inner conductor' carrying current in the opposite direction. On the other hand, the 'surface conductor' is exposed to more perpendicular magnetic field mainly due to weak cancellation of perpendicular magnetic field components between the
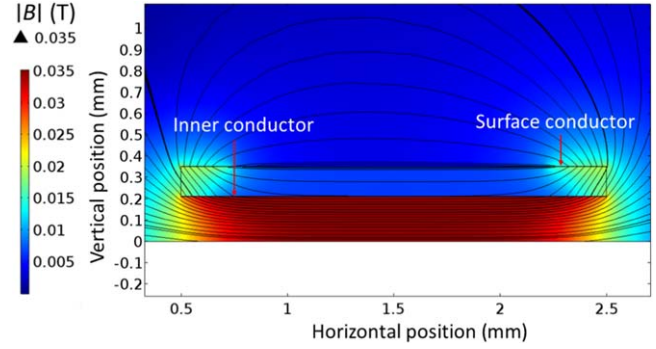
Figure 17. Magnetic field distribution around the 'surface conductor' and the 'inner conductor' in TPBS at $I_{t,turn}/I_{c0,cable} = 0.7$.

other 'surface conductor' carrying current in the opposite direction. Therefore, $L + M_{13} - M_{12} - M_{23} < L + M_{24} - M_{21} - M_{14}$ and hence $I_1 < I_2$. However, when I_2 (the current in the 'inner conductor') is close to the strand I_c in the RBS as shown in figure 15, R_2 suddenly appears according to the E–J relationship. As a result, I_2 starts to be saturated, and V becomes larger due to the appearance of V_{R_2}. Larger V in turn increases I_1 according to the following equation, where R_1 is still zero, and I_2 stays at approximately the same value

$$
I_1 = \frac{V - j\omega(M_{12} - M_{13})I_2}{R_1 + j\omega(L_1 - M_{14})}. \tag{9}
$$

Eventually the I_1 and I_2 values converge with increasing I value as shown in figure 15. In this dynamic process, the transverse resistance between the conductors is assumed to be infinite or very large, and unlike the small transverse resistance found in non-insulated coils [37]. Roebel strands punched from stabilized HTS wires and stabilized HTS wires are normally oxidized through exposure to the atmosphere, and are expected to have very large transverse contact resistance [36]. Therefore, the numerical result here will be representative of RBSs and TPBSs where multiple bare strands/wires are in contact.

To better understand the effect of equal and unequal current distributions on AC loss, figures 18 and 19 compare the distribution profiles of current density, magnetic field density, electric field, and loss power density of the 'surface conductors' and 'inner conductors' in the RBS and TPBS when $I_{t,turn}/I_{c0,cable} = 0.3$ and 0.7 at 27.74 Hz. The results shown here are for peak current values when $\omega t = 3\pi/2$. Figure 18 shows the result for $I_{t,turn}/I_{c0,cable} = 0.3$ and figure 19 shows the result for $I_{t,turn}/I_{c0,cable} = 0.7$, respectively.

When $I_{t,turn}/I_{c0,cable} = 0.3$, more current flows in the 'inner conductor' than the 'surface conductor' in the TPBS as shown in figure 15. As a result, the 'surface conductor' in the TPBS carries less current than the 'surface conductor' in the RBS. Hence, the saturated region of the current density for the 'surface conductor' in the TPBS extends to shallower region of the conductor than that of the RBS, and it leads to less penetration depth of the magnetic field to the conductor as shown in figures 18(a) and (b). Shallower magnetic field penetration leads to generation of electrical field in a shallower region, and causes less AC loss in the 'surface
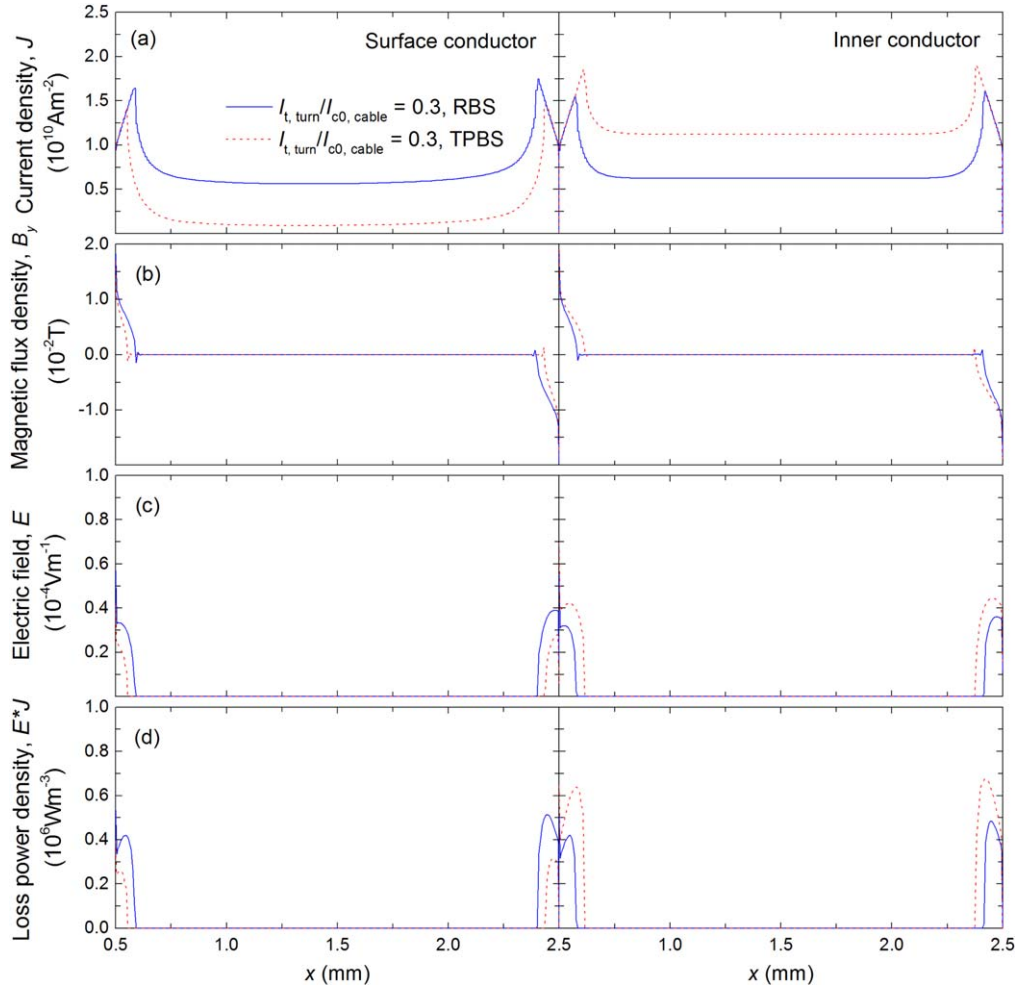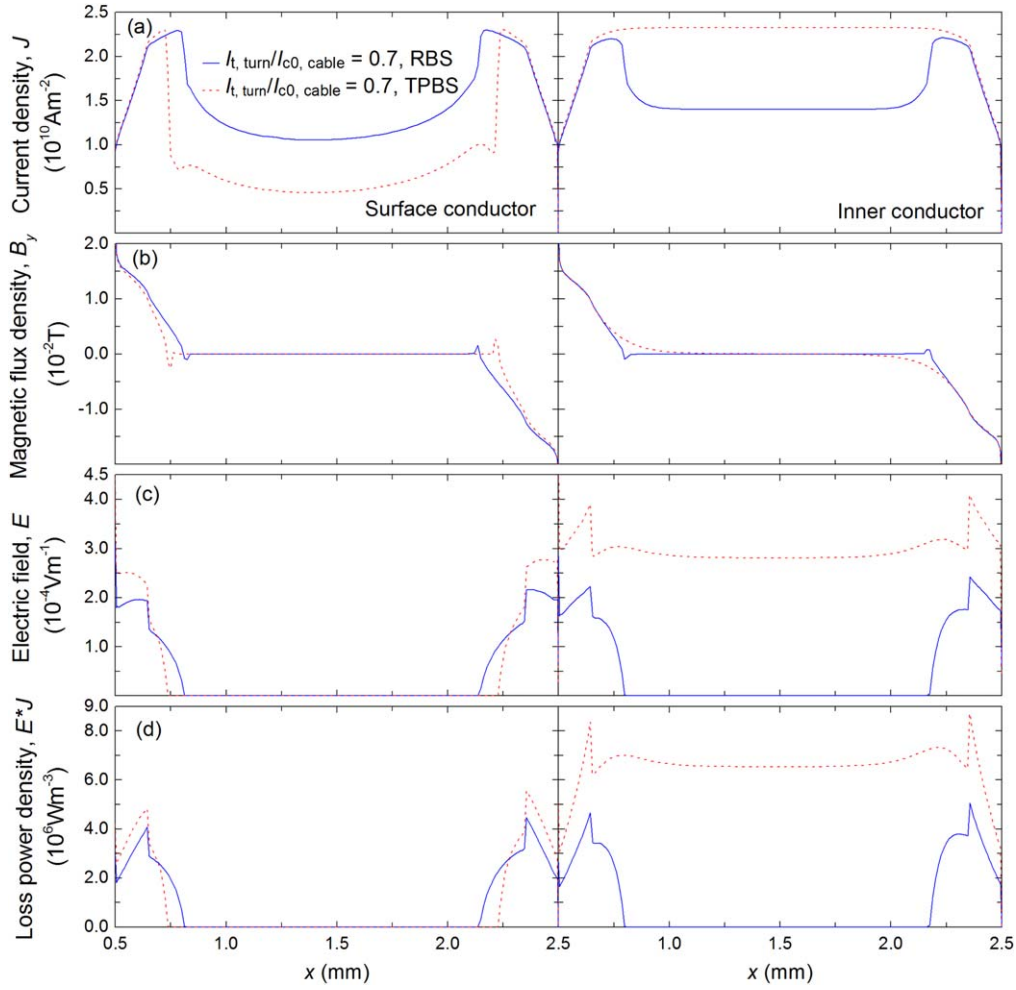
Figure 18. The distribution profiles of current density, magnetic field density, electric field, and loss power density of the 'surface conductor' and the 'inner conductor' in the RBS and TPBS when $\omega t = 3\pi/2$ and $I_{t,turn}/I_{c0,cable} = 0.3$ (a) current density distribution, (b) magnetic field distribution, (c) electric field distribution, (d) loss power density distribution.

conductor' of the TPBS than that of RBS as shown in figures 18(c) and (d). On the other hand, the 'inner conductor' in the TPBS carries more current than the 'inner conductor' in the RBS. In this case, the opposite holds true for the 'inner conductors' of the TPBS and RBS. More AC loss is generated in the 'inner conductor' of the TPBS than that of the RBS. Eventually, at $I_{t,turn}/I_{c0,cable} = 0.3$, overall AC loss values in the RBS and TPBS are competitive as evident in figure 17(d).

When $I_{t,turn}/I_{c0,cable} = 0.7$, the 'surface conductors' for both the TPBS and RBS behave similarly to that when $I_{t,turn}/I_{c0,cable} = 0.3$, even though the saturated region of current density in the conductors extends deeper due to larger I. There are some differences in penetration depths, generated E and loss power density profiles in the 'surface conductors'. However, the overall behaviors are similar to those in the 'surface conductors' shown in figures 18(b)–(d). Interestingly, however, there are distinctive differences between the current density profiles in the 'inner conductors' of the TPBS and RBS as shown in figure 19(a). While 'inner conductor' in the RBS remains in typical saturation and subcritical regions [38], the 'inner conductor' in the TPBS behaves very differently, i.e. the J values in the central region of the conductor

are even bigger than J_c which means the conductor is in the flux flow regime. As a result, conductor is fully penetrated and a large electrical field (more than three times $E_c = 1\,\mu V\,cm^{-1}$) is generated in the whole conductor width. Therefore, loss generation occurs in whole conductor width, leading to higher AC loss compared to the 'inner conductor' of the RBS.

Transport AC losses in the RBS, TPBS, and EBS at 27.74 Hz are plotted as a function of $I_{t,turn}/I_{c0,cable}$, in figure 20. AC loss values in the RBS are slightly smaller than those in the TPBS and EBS at low current amplitues, but much smaller when $I_{t,turn}/I_{c0,cable} > 0.6$. At $I_{t,turn}/I_{c0,cable} = 0.3$, the AC loss was reduced from 1.11×10^{-5} J/m/cycle/cable in TPBS to 1.00×10^{-5} J/m/cycle/cable in the RBS, corresponding to 10% reduction, whilst at $I_{t,turn}/I_{c0,cable} = 0.7$, the AC loss was reduced from 5.82×10^{-4} J/m/cycle/cable in TPBS to 2.05×10^{-4} J/m/cycle/cable in RBS, corresponding to 65% loss reduction. The AC loss values in the EBS agree approximately with those in the TPBS. It is worth noting that the EBS can be regarded as two parallel stacks (two 2 mm wide four conductors) with zero horizontal gap between the conductors [36]. The result clearly implies that continuously transposed

9

Figure 19. The distribution profiles of current density, magnetic field density, electric field, and loss power density of the 'surface conductor' and the 'inner conductor' in the RBS and TPBS when $\omega t = 3\pi/2$ and $I_{t,turn}/I_{c0,cable} = 0.7$ (a) current density distribution, (b) magnetic field distribution, (c) electric field distribution, (d) loss power density distribution.
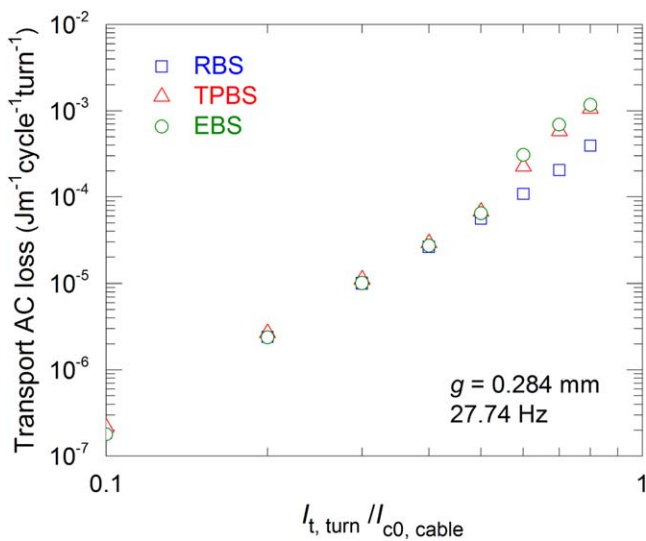
Figure 20. Comparison of calculated AC loss results calculated in the RBS with $g = 0.284$ mm, TPBS, and EBS at 27.74 Hz.

Roebel cables are much more advantagous than non-transposed simple vertical stacks when operated at high current amplitudes.

4. Conclusions

We demonstrated that transport AC loss in a 4/2 (four 2 mm strands) Roebel cable can be measured in serial connection using only one voltage loop attached to a strand. Based on this result, we carried out, for the first time, transport AC loss measurements in two bifilar 4/2 Roebel cable stacks (RBSs) with different vertical spacing between the turns by serial connection using only two voltage loops attached to each strand in each turn of the stacks. The results were compared with the AC loss calculated for 2D FEM models using the *H*-formulation including non-uniform lateral J_c distribution. The simulated results in RBS were compared with the simulated results in two parallel bifilar stacks (TPBS) which have the same geometrical dimensions but have unequal current distribution between the

conductors composing the stacks and also with the calculated AC loss results in an equivalent bifilar stack (EBS) comprising four 4 mm wide conductors with identical vertical geometrical dimensions to the RBS with smaller spacing but non-uniform current sharing between the conductors.

Transport AC loss values in the RBS with $g = 0.284$ mm are much smaller compared to that in the straight $4/2$ Roebel cable due to cancellation of the perpendicular magnetic field components between the upper and lower turns. AC loss increases with increasing spacing between upper and lower halves of the RBS. Simulation results show that variation in spacing ranging from 0.16–1.26 mm produces more than three times difference in the AC loss.

The calculated transport AC loss values in RBS with $g = 0.284$ mm agree approximately with those both in TPBS and EBS until $I_{t,turn}/I_{c0,cable}$ is around 0.5, but are approximately three times those in TPBS and EBS when $I_{t,turn}/I_{c0,cable} > 0.6$. This is a result of the unequal current distribution between the conductors composing the TPBS and EBS. When $I_{t,turn}/I_{c0,cable} > 0.6$, the 'inner conductors' in the TPBS and EBS carries more current than the critical current of the conductors leading to flux flow which in turn leads to larger AC loss in the TPBS and EBS. The results imply that transposed Roebel cables should be used for high current operation compared to simple non-transposed vertical stacks which have non-uniform current distribution. This work is the first numerical demonstration of the advantage of Roebel cable over non-transposed vertical stacks due to equal current sharing between strands as compared with unequal current sharing.

The results obtained in this work have practical implication for bifilar coil windings in SFCL applications.

ORCID iDs

Zhenan Jiang ⓘ https://orcid.org/0000-0002-3482-3510
Rodney A Badcock ⓘ https://orcid.org/0000-0003-0219-9570

References

[1] Clem J R 2008 *Phys. Rev.* B **77** 134506
[2] Schmidt W, Gamble B, Kraemer H P, Madura D, Otto A and Romanosky W 2009 *Supercond. Sci. Technol.* **23** 014024
[3] Elschner S *et al* 2012 *Physica* C **482** 98–104
[4] Weiss J D, Mulder T, ten Kate H J and van der Laan D C 2016 *Supercond. Sci. Technol.* **30** 014002
[5] van der Laan D C, Noyes P D, Miller G E, Weijers H W and Willering G P 2013 *Supercond. Sci. Technol.* **26** 045005
[6] Šouc J, Vojenčiak M and Gömöry F 2012 *Supercond. Sci. Technol.* **23** 045029
[7] Takayasu M, Chiesa L, Bromberg L and Minervini J V 2011 *Supercond. Sci. Technol.* **25** 014011
[8] Ogawa J, Fukui S, Oka T, Sato T, Shinkai K, Koyama T and Ito T 2010 *IEEE Trans. Appl. Supercond.* **20** 1300–3
[9] Jiang Z, Amemiya N, Kakimoto K, Iijima Y, Saitoh T and Shiohara Y 2008 *Supercond. Sci. Technol.* **21** 015020
[10] Song W, Jiang Z, Zhang X, Staines M, Bumby C W, Badcock R and Fang J 2018 *IEEE Trans. Appl. Supercond.* **28** 5900606
[11] Terzieva S, Vojenčiak M, Pardo E, Grilli F, Drechsler A, Kling A, Kudymow A, Gömöry F and Goldacker W 2009 *Supercond. Sci. Technol.* **23** 014023
[12] Jiang Z *et al* 2010 *Supercond. Sci. Technol.* **23** 025028
[13] Goldacker W, Grilli F, Pardo E, Kario A, Schlachter S I and Vojenčiak M 2014 *Supercond. Sci. Technol.* **27** 093001
[14] Long N J, Badcock R A, Hamilton K, Wright A, Jiang Z and Lakshmi L S 2010 *J. Phys.: Conf. Ser.* **234** 022021
[15] Amemiya N, Jiang Z, Li Z, Nakahata M, Kato T, Ueyama M, Kashima N, Nagaya S and Shiohara S 2008 *Physica* C **468** 1718–22
[16] Iwakuma M *et al* 2009 *Physica* C **469** 1726–32
[17] Stavrev S, Grilli F, Dutoit B and Ashworth S P 2005 *Supercond. Sci. Technol.* **18** 1300–12
[18] Grilli F and Pardo E 2010 *Supercond. Sci. Technol.* **23** 115018
[19] Jiang Z, Staines M, Badcock R A, Long N J and Amemiya N 2009 *Supercond. Sci. Technol.* **22** 095002
[20] Yang Y, Hughes T, Beduz C, Spiller D M, Scurlock R G and Norris W T 1996 *Physica* C **256** 378–86
[21] van der Laan D C and Ekin J W 2008 *Supercond. Sci. Technol.* **21** 115002
[22] Nguyen D N, Grilli F, Ashworth S P and Willis J O 2009 *Supercond. Sci. Technol.* **22** 055014
[23] Hong Z, Campbell A M and Coombs T A 2006 *Supercond. Sci. Technol.* **19** 1246–52
[24] Rodriguez-Zermeno V M, Mijatovic N, Træholt C, Zirngibl T, Seiler E, Abrahamsen A B, Pedersen N F and Sorensen M P 2011 *IEEE Trans. Appl. Supercond.* **21** 3273–6
[25] Brambilla R, Grilli F and Martini L 2007 *Supercond. Sci. Technol.* **20** 16–24
[26] Kim Y B, Hempstead C F and Strnad A R 1962 *Phys. Rev. Lett.* **9** 306–9
[27] Jiang Z, Thakur K P, Staines M, Badcock R A, Long N J, Buckley R G, Caplin A D and Amemiya N 2011 *Supercond. Sci. Technol.* **24** 065005
[28] Higashikawa K, Guo X, Inoue M, Jiang Z, Badcock R, Long N and Kiss T 2017 *IEEE Trans. Appl. Supercond.* **27** 8001404
[29] Nishioka T, Amemiya N, Enomoto N, Jiang Z, Yamada Y, Izumi T, Shiohara Y, Saitoh T, Iijima Y and Kakimoto K 2005 *IEEE Trans. Appl. Supercond.* **15** 2843–6
[30] Jiang Z, Amemiya N, Maruyama O and Shiohara Y 2007 *Physica* C **463** 790–4
[31] Šouc J, Gömöry F and Vojenčiak M 2012 *Supercond. Sci. Technol.* **25** 014005
[32] Zermeño V M, Habelok K, Stępień M and Grilli F 2017 *Supercond. Sci. Technol.* **30** 034001
[33] Amemiya N, Tsukamoto T, Nii M, Komeda T, Nakamura T and Jiang Z 2014 *Supercond. Sci. Technol.* **27** 035007
[34] Goldacker W, Frank A, Kudymow A, Heller R, Kling A, Terzieva S and Schmidt C 2009 *Supercond. Sci. Technol.* **22** 034003
[35] Norris W T 1970 *J. Phys. D: Appl. Phys.* **3** 489–507
[36] Jiang Z, Staines M, Long N J, Badcock R A, Bumby C, Talantsev E, Hamilton K, Buckley R G and Amemiya N 2014 *Supercond. Sci. Technol.* **27** 075007
[37] Hahn S, Radcliff K, Kim K, Kim S, Hu X, Kim K, Abraimov D V and Jaroszynski J 2016 *Supercond. Sci. Technol.* **29** 105017
[38] Zeldov E, Clem J R, McElfresh M and Darwin M 1994 *Phys. Rev.* B **49** 9802–22